Innovations in Renewable Energies Offshore – Guedes Soares & Wang (Eds)

Numerical modelling of the DTU-OWC wave energy device - COER solution

H.A. Said & J.V. Ringwood
Centre for Ocean Energy Research (COER), Department of Electronic Engineering, Maynooth University Maynooth, Co. Kildare, Ireland

T. Kelly
Centre for Renewable Energy, Dundalk IT, Ireland

ABSTRACT: In this work, the focus is on a small-scale (1:50) measurements of a single, Oscillating Water Column (OWC) chamber mounted on one side of a wave flume so that the chamber opening faces the opposite side of the flume. A Single-Degree-of-Freedom (1-DoF), time-domain numerical model of the DTU OWC is first developed. The model is based on the well-known Cummins equation, and uses Boundary Element Method (BEM) software codes to determine the necessary hydrodynamic and hydrostatic parameters. The time-domain model is simulated in MATLAB as a set of Ordinary Differential Equations (ODEs) in matrix (or state space-like) form, which are solved using the ODE solvers available in MATLAB. The model is simulated for both two-way and one-way absorption scenarios. A bang-bang strategy is used to model the one-way valve. The results indicate that the time-domain model matches the experimental data well for two-way absorption scenarios but has difficulties with the one-way absorption scenarios.

1 INTRODUCTION

The transition to a low-carbon economy, and combating anthropogenic climate change on a global scale, necessitates the adoption of renewable energy alternatives. Renewable energy sources are pivotal in this endeavour, as they offer sustainable solutions by harnessing naturally replenished resources without generating greenhouse gases. Among these sources, wave energy stands out for its vast potential to provide clean energy (Reguero et al. 2015). However, it remains relatively untapped compared to other renewables due to a higher Levelised Cost of Energy (LCoE).

Wave Energy Converters (WECs) represent a promising segment within the global renewable energy landscape. However, to compete effectively with offshore wind and solar power, the WEC sector must demonstrate the reliability of its prototypes, which involves deploying dependable demonstration models, serving as a precursor to scaled-up commercialisation and the realisation of economies of scale. Achieving this transition requires access to accurate and dependable numerical modelling tools. These tools play a crucial role in evaluating performance metrics during the initial design phases (Dallman et al. 2018), ensuring the efficiency and viability of wave energy conversion systems. In this regard, the International Energy Agency (IEA) Technology Collaboration Programme for Ocean Energy Systems (OES) (IEA 2022) has been active since 2001, focusing on facilitating the commercialisation of WECs. The OES Working Group on Wave Energy Modelling was established, and as part of this initiative, OES Task 10 was launched in 2016. This task is dedicated to the numerical modelling and verification of Wave Energy Converter (WEC) systems, aiming to evaluate the accuracy and reliability of numerical models across all stages of WEC development. This paper describes the work carried out by The Centre for Ocean Energy Research at Maynooth University (MU), Ireland, in association with the Centre for Renewable Energy at Dundalk IT (DkIT), Ireland, regarding the OES Task 10: Numerical modelling and verification. As part of OES Task 10, several modelling exercises have been completed over the past few years (Wendt et al. 2019, Bingham et al. 2021, Kramer et al. 2021).

This paper is part of the next stage of OES Task 10, which aims to model a fixed OWC chamber with two-way and one-way energy absorption. Typically, OWCs are equipped with self-rectifying turbines, which rotate in one direction regardless of the bidirectional airflow. In the OWC modelled herein, however, an alternative strategy is employed, which utilises a unidirectional passive valve that allows only one-way venting, leading to power absorption in one direction (up-stroke or down-stroke), depending upon the configuration of the passive valve. The experimental tests were conducted in the Technical University of Denmark (DTU), and the free surface elevation data was provided to the participating teams. This modelling exercise is blind since the participating teams do not have access to the experimental results before submission of their

DOI: 10.1201/9781003558859-27

modelling results. However, the experimental data was made available after the submission of the modelling results, which is used for comparison in Section 4.

In this paper, a Single-Degree-of-Freedom (1-DoF) time-domain numerical model for the DTU OWC is presented. The model assumes the water column acts only in pumping mode. Furthermore, the proposed time-domain model is adapted for the one-way absorption cases to simulate a one-way passive valve in line with the experimental results. In particular, a so-called *bang-bang* strategy is employed to model the effect of the one-way valve (Kelly 2018).

The remainder of the paper is organised as follows: Section 2 provides a brief overview of the experimental setup and testing conditions, while Section 3 presents the time-domain model developed by the MU-DkIT team, including thermodynamic representation, hydrodynamic calculations, and parametric approximations utilised to achieve the final model. Results are presented in Section 4, while Section 5 concludes this study.

2 THE EXPERIMENTAL SET-UP

The results obtained from the experimental measurements are briefly outlined here, with comprehensive details available in (Joensen et al. 2023). Figure 1 illustrates the dimensions and layout of Flume 1 at the DTU hydraulics laboratory. This flume spans 25 [m] in length and 0.6 [m] in width and maintains a water depth of $h = 0.65$ [m]. In Figure 1, the single chamber model is affixed to one flume wall, acting as the plane of symmetry, while the water column is laterally activated by passing waves. The origin of the coordinate system is positioned at the chamber centre along the tank wall, with the z-axis extending upwards from the still water level.

A series of monochromatic incident wave conditions were tested, as detailed in Table 1. Here, T represents the wave period, λ signifies the wavelength and $H = 2A$ denotes the height, with A referring to the wave amplitude. H_1 and H_2 correspond to wave steepness values of $\varepsilon = H/\lambda = [0.025, 0.04]$, respectively, indicating nearly linear conditions. Data was collected at a rate of 512 [Hz], extending up to $t_{\max}$. This duration represents the time the wavefront takes to travel from the wavemaker to the beach and back to the chamber, based on the linear group velocity. Limiting the record to this duration prevents any potential reflections from the beach. For each wave condition outlined in Table 1, initial runs were conducted without the chamber in the tank to establish the undisturbed incident wave conditions, which are given to each team to test their models. Subsequently, the chamber was introduced into the tank, and each wave condition was tested under various scenarios: with the chamber open (no PTO damping), with two-way energy absorption, with up-stroke venting, and with down-stroke venting. A one-way passive valve is used implement up-/down-stroke venting cases.

Table 1. Monochromatic wave conditions tested in the experiments. The highlighted green row represent the resonance period of the scaled-OWC.

T (s)	λ (m)	H_1 (m)	H_2 (m)	$t_{\max}$ (s)
0.57	0.51	0.013	0.021	84
0.74	0.85	0.021	0.034	65
0.78	0.94	0.024	0.038	62
0.79	0.98	0.025	0.039	60
0.81	1.02	0.026	0.041	59
0.82	1.05	0.026	0.042	58
0.83	1.07	0.027	0.043	58
0.84	1.11	0.028	0.044	57
0.86	1.15	0.029	0.046	55
0.90	1.26	0.032	0.050	52
0.98	1.49	0.037	0.060	47
1.15	1.98	0.050	0.079	38
1.31	2.48	0.062	0.099	32
1.47	2.98	0.074	0.119	27
1.64	3.46	0.087	0.138	24

3 TIME-DOMAIN NUMERICAL MODEL

3.1 *Thermodynamic representation*

An OWC may be considered as comprising two coupled subsystems, a hydrodynamic system which describes the behaviour of the water column, and a thermodynamic system, which describes the behaviour of the air volume above the water column. The two subsystems are coupled through the motion of the water column. This motion pressurises and depressurise the air, and the force resulting from the change of air pressure, which acts over the surface of the water column.

An expression to describe the coupling of the variation of the air pressure within the volume above the water column in the chamber, with respect to the mass flow of air into or out of the chamber, and the variation in the water column height within the chamber, can be obtained by considering the First Law of Thermodynamics, the internal energy of the system and the rate at which work is done by the system. The following expression for the rate of change of pressure in the volume of air trapped in the OWC chamber above the water column, in terms of the mass flow of air into or out of the chamber and the changing volume of the air may be obtained (Kelly 2018):

$$\dot{p}(t) = \frac{c_s^2}{V(t)}\dot{m}(t) - \frac{\gamma p(t)}{V(t)}\dot{V}(t), \qquad (1)$$

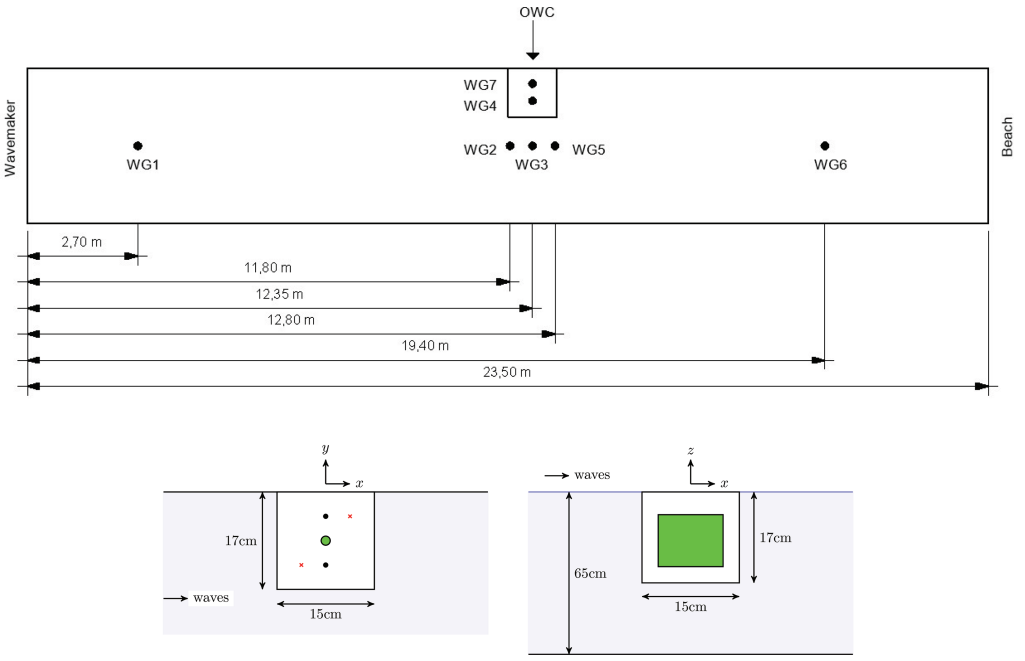

Figure 1. Layout of the experiments and the chamber. In the bottom left panel, the green circle represents the orifice, the blue dots indicate WG7 & WG4, and the red crosses mark the locations of the pressure sensors in the chamber lid (Joensen et al. 2023).

where $p(t)$ is the air pressure within the OWC chamber as it varies with time, c_s in the speed of sound in air, $V(t)$ is the volume of air in the OWC chamber as it varies with time, $\dot{m}(t)$ is the time varying mass flow rate into, or out of, the chamber and γ, the adiabatic index, is approximately 1.4 for air.

Assuming a uniform cross-section, the volume of air in the chamber is given by:

$$V = A_{owc}[h_o - u_7(t)], \tag{2}$$

where A_{owc} is the cross-sectional area of the water column and $u_7(t)$ is the vertical displacement of the water column in pumping mode. By differentiating (2) with respect to time, the rate of change of the air volume is given by:

$$\dot{V} = -A_{owc}\dot{u}_7. \tag{3}$$

3.2 *Water column hydrodynamics*

The equations of motion for the water column in 1-DoF, including the effect of variations in air pressure acting on the surface of the water column, are described in Section 3.3. The frequency-dependant hydrodynamic parameters, such as the added mass, radiation damping and exciting force are generally obtained using BEM codes, such as WAMIT (Wamit® 2012) or NEMOH (NEMOH 2017) . WAMIT V7 is used to generate the hydrodynamic parameters for the results presented herein. The distinguishing characteristic of the model described herein, compared to other models which form part of the OES Task, is the *absence* of tank walls in the model. In order to investigate the impact of the tank walls on the behaviour of the OWC, the OWC chamber is modelled in three dimensional space, in the absence of tank walls, and hence the effects of side-wall reflections are not included. The importance of including side-wall reflections may then be assessed by comparing the results of the model described herein to results obtained from models which include such reflections, although such a comparison is not the subject of this paper. The geometry of the wetted surfaces of the OWC was defined using Multisurf (Aerohydro Inc. 2011), a surface CAD modelling tool, where an object is represented by drawing the exterior surfaces of the object. The free surface of the water column is included in this model, and using the generalised modes routine within WAMIT, the hydrodynamics of the water column are modelled as those of an infinitely thin, massless disk located at the free surface in the manner proposed by Evans (Evans 1978). The Multisurf model used to estimate the hydrodynamic parameters is shown in Figure 2.

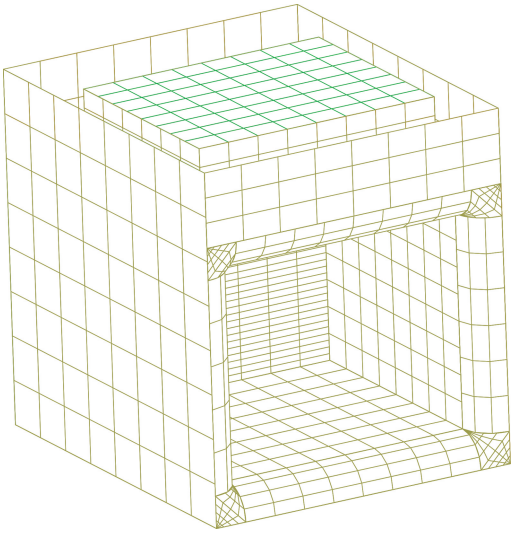

Figure 2. Illustration of the single chamber OWC geometry used in the time-domain model.

3.3 *Time-domain modelling*

A 1-DoF model of the water column, which operates under the assumption that the water column acts in pumping mode only (referred to as mode 7), is developed. Note that the first sloshing mode of the water column does not change the pressure in the air above the water column and, therefore, does not contribute to the power absorbed by the OWC. Furthermore, the hydrodynamic coupling between the pumping and sloshing modes is found to be several orders of magnitude lower than the pumping mode hydrodynamics, and thus it was considered that the coupling between the two modes may be neglected. The equation of motion of the water column for 1-DoF in the time-domain, neglecting non-linear terms, is given by:

$$a_{77}^{\infty}\ddot{u}_7(t) + \int_{-\infty}^{t} kr_7(t-\tau)\dot{u}_7(\tau)d\tau + c_{77}u_7(t) + p(t)A_{owc} = fe_7(t), \tag{4}$$

where a_{77}^{∞} is the infinite frequency added mass for mode 7, $kr_7(t)$ is the impulse response function for the radiation forces, c_{77} is the coefficient of buoyancy for mode 7, $p(t)$ the absolute pressure in the air chamber as defined by (1), fe_7 the exciting force in mode 7, and u_7, $\dot{u}_7$ $\ddot{u}_7$ are the vertical displacement, velocity and acceleration of the water column, respectively. Equation (4) is a modified version of Cummins' Equation (Cummins 1962).

As indicated by (1), the variation in air pressure within the OWC chamber depends on the mass flow rate of air, $\dot{m}$, into and out of the chamber through an orifice (two-way absorption). The direction of the flow, either into or out of the chamber, depends on the value of p. If $p > 0$, then air flows from the chamber to the atmosphere, and $\dot{m}$ in (1) is negative, whereas if $p < 0$, air flows from the atmosphere into the chamber, and $\dot{m}$ is considered positive. If $p = 0$, no airflow occurs. Orifice theory (ISO 2022) is used to model these conditions, as shown in Table 2.

Table 2. Mass flow equations for DTU-OWC for two-way absorption.

Case	Mass flow
$p>0$	$\dot{m} = -Cd_O A_{ori}\sqrt{2\rho_{air}\lvert p - p_{atmos}\rvert}$
$p<0$	$\dot{m} = Cd_O A_{ori}\sqrt{2\rho_{air}\lvert p_{atmos} - p\rvert}$
$p = 0$	$\dot{m} = 0$

In Table 2, $\dot{m}$ represents mass flow rate through the orifice. Cd_O and A_{ori} denote coefficient of discharge and cross-sectional area for the orifice, while ρ_{air} is the density of air.

We now recast coupled Equations (1) and (4) in state-space-like form. Such a form will facilitate the later replacement of the convolution term with a state-space approximation. Denoting the vector of state variables as X, and the i^{th} entry of X as x_i, the chosen state variables are:

$$x_1 = u_7, \quad x_2 = \dot{u}_7, \quad x_3 = p. \tag{5}$$

From (4) and (1), it can be shown that:

$$\dot{x}_1 = \dot{u}_7 = x_2, \tag{6}$$

$$\dot{x}_2 = \ddot{u}_7 = \frac{fe_7}{a_{77}^{\infty}} - \frac{\int_0^t kr_7(t-\tau)\dot{u}_7(\tau)dt}{a_{77}^{\infty}} - \frac{c_{77}}{a_{77}^{\infty}}x_1 - \frac{A_{owc}}{a_{77}^{\infty}}x_3, \tag{7}$$

$$\dot{x}_3 = \dot{p} = \frac{c_s^2}{V}\dot{m} - \gamma\frac{p}{V}\dot{V} = \frac{c_s^2}{A_{owc}[h_o - x_1]}\dot{m} + \frac{\gamma(x_3 + p_{atmos})}{[h_o - x_1]}x_2. \tag{8}$$

For clarity, the convolution integral is replaced in future equations with the notation *conv*, hence $conv = \int_0^t kr_7(t-\tau)\dot{u}_7(\tau)dt$. For a 1-DoF model of the DTU-OWC, (6), (7) and (8) are assembled into a state-space form to yield:

$$\overbrace{\begin{pmatrix}\dot{x}_1\\ \dot{x}_2\\ \dot{x}_3\end{pmatrix}}^{\dot{X}} = \overbrace{\begin{pmatrix}0 & 1 & 0\\ -\frac{c_{77}}{a^{\infty}_{77}} & 0 & -\frac{A_{owc}}{a^{\infty}_{77}}\\ 0 & \frac{\gamma(x_3+p_{atmos})}{[h_o-x_1]} & 0\end{pmatrix}}^{A} \overbrace{\begin{pmatrix}x_1\\ x_2\\ x_3\end{pmatrix}}^{X}$$

$$+ \overbrace{\begin{pmatrix}0 & 0\\ (fe_7 - conv) & 0\\ 0 & \frac{c_x^2}{A_{owc}[h_o-x_1]}\end{pmatrix}}^{B} \overbrace{\begin{pmatrix}\frac{1}{a^{\infty}_{77}}\\ \dot{m}\end{pmatrix}}^{U}, \qquad (9)$$

where $\dot{m}$ is determined from Table 2 at each time step as appropriate.

3.4 *Parametric approximation of radiation kernel*

The state space model presented in (9) contains a convolution term which accounts for the radiation forces. This convolution term is computationally inefficient due to the large number of calculations that must be performed for each time step in the simulation and the need for small time steps to obtain sufficiently good accuracy. To enhance computational efficiency, it is typical to substitute this convolution term with a state-space approximation using various toolboxes (Perez and Fossen 2008, Pena-Sanchez et al. 2019). In the following, the procedure used to obtain the parametric approximation of radiation kernel for DTU-OWC is detailed.

3.4.1 *Added mass reconstruction*

As discussed in Section 3.2, WAMIT determines the hydrodynamic parameters of a water column by modelling the free surface as an infinitely thin, mass-less disc. However, challenges arise when employing WAMIT to model the added mass of thin elements at high frequencies. The expected trend of the added mass versus frequency curve should approach the infinite frequency added mass asymptotically at high frequencies. Nevertheless, for the thin disc representing surface of the water column, WAMIT results tend towards negative infinity for the pumping mode and either negative or positive infinity for coupled modes. Additionally, the accuracy of the obtained infinite frequency added mass value is often compromised and can vary significantly depending on the WAMIT version used (Kelly et al. 2022). Consequently, frequency-dependent added mass values are 'reconstructed' from the radiation damping values before integration with an approximating toolbox, the FOAMM toolbox (Pena-Sanchez et al. 2019) in this case, to derive a parametric approximation of radiation convolution term. If the values of added mass, obtained directly from WAMIT, are used as input to the FOAMM toolbox to obtain approximations to the IRF of the radiation force, the result obtained for the approximation is inaccurate, and, in some cases, unstable. An approach used by the authors previously to overcome the issue with added mass is described in (Kelly et al. 2015), based on the fact that added mass and radiation damping are related to each other through the Kramers-Kronig (Newman and Grue 2018) or Ogilvie (Ogilvie 1964) relations, which may also be considered expressions of the Hilbert transformation. These relationships are given by:

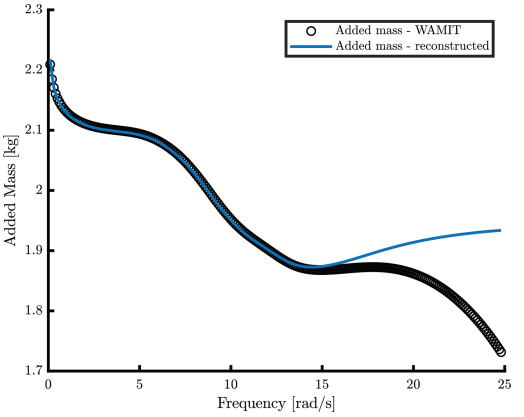

Figure 3. Added mass versus frequency results calculated directly by WAMIT and the reconstructed added mass for the DTU-OWC.

$$a_{77}(\omega) = a^{\infty}_{77} - \frac{1}{\omega}\int_0^{\infty} kr_7(t)\sin(\omega t)dt, \qquad (10)$$

and,

$$b_{77}(\omega) = \int_0^{\infty} kr_7(t)\cos(\omega t)dt. \qquad (11)$$

Once values for $b_{77}(\omega)$ are known, and the appropriate value of a^{∞}_{77} determined, $a_{77}(\omega)$ can be 'reconstructed' from the radiation damping values by creating $kr_7(t)$ from the $b(\omega)$ vector. Figure 3 illustrates a comparison between the added mass versus frequency curves for the added mass values calculated directly by WAMIT and the 'reconstructed' added mass curve at low frequencies for the DTU-OWC. Note that the value of a^{∞}_{77} obtained using this method and the corresponding value provided by the OES team using a different approach are virtually identical.

3.4.2 *Parametric approximation through FOAMM*

In this study, the FOAMM toolbox (Pena-Sanchez et al. 2019), developed at the Centre for Ocean Energy Research (COER), Maynooth University, is used for the parametric approximation of the radiation kernel. The toolbox uses a moment-matching system identification algorithm (Faedo et al. 2018). The input to the FOAMM toolbox is the WAMIT data in the form of

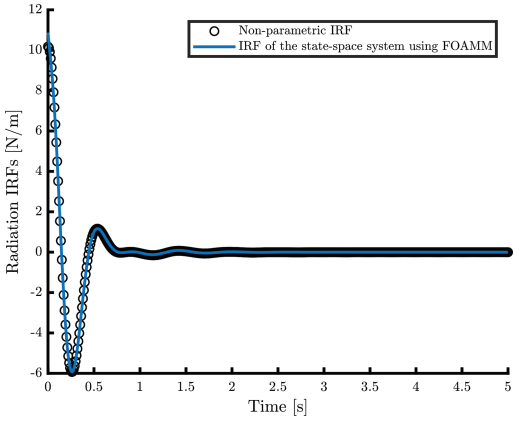

Figure 4. A comparison of IRF of parametric state space approximation calculated utilising FOAMM versus non-parametric radiation IRF for a 1-DoF DTU-OWC.

radiation damping, frequency, and (reconstructed) added mass vectors for a given mode of motion (mode 7 in the case of the 1-DoF model). Furthermore, the added mass at infinite frequency is also required. If the infinite frequency added mass is not supplied by the user, the toolbox will automatically estimate the added mass at infinity using Ogilvie's relation.

The FOAMM toolbox returns a state space approximation in the following form:

$$\begin{aligned} \dot{X}_r(t) &= A_r X_r(t) + B_r u_r(t), \\ y_r(t) &= C_r X_r(t) \approx \int_0^t k r_7(t-\tau)\dot{u}_7(t)d\tau, \end{aligned} \tag{12}$$

where A_r, B_r and C_r are the matrices from the parametric approximation of the radiation kernel. In the current work, the best fit between the non-parametric WAMIT IRF and the approximated IRF through FOAMM is achieved by selecting three frequencies for an exact match, which results in an approximation of order six, illustrated by the IRF comparison shown in Figure 4.

Using the parametric approximation of the radiation kernel explained in Section 3.4.2, the order of the state space system in (9) is increased by the order of the radiation approximation, i.e. six in this case.

3.5 *One-way valve implementation*

As discussed in Section 2, the DTU-OWC employs a one-way passive valve to implement one-way (up-stroke or down-stroke) absorption. A *bang-bang* strategy, inspired by the bang-bang control mechanism in control theory, in which the manipulated control variable switched abruptly between two states, is used to model such a passive valve. For a description of the theory behind *bang-bang* strategies see, for example, (Sonneborn and Van Vleck 1964). In this mechanism, the chamber gauge pressure is manually set to zero depending on the direction of the water column (up-stroke/down-stroke venting), as illustrated in Figure 5 for up-stroke venting.

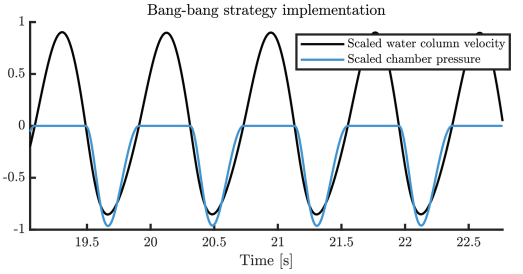

Figure 5. Bang-bang strategy implementation for up-stroke venting case of the one-way passive valve.

Table 3. Mass flow equations for DTU-OWC for one-way (up-stroke) venting.

if $\dot{u}_7 < 0$: **Direction of the water column is down and valve is closed**.	
Case	Mass flow
$p < 0$	$\dot{m} = Cd_O A_{ori}\sqrt{2\rho_{air}\lvert p_{atmos} - p\rvert}$
$p > 0$	$\dot{m} = 0$
$p = 0$	$\dot{m} = 0$
else $\dot{u}_7 >= 0$**: Direction of the water column is up and valve is open.**	
$p = 0$	$\dot{m} = -A_{owc}\rho_{air}\dot{u}_7$

The mass flow equations, in this case, are updated in the time-domain model. For instance, Table 3 details the implementation of the up-stroke venting case, showing that the mass flow condition changes depending on the direction of the water column. While the same approach is applied to model down-stroke venting, it is not included here for brevity.

4 RESULTS

In order to implement the models detailed in Section 3, knowledge of excitation forces, $fe_7(t)$, is required. The excitation force, for mode 7 in the time-domain, can be represented by the following convolution integral:

$$fe_7(t) = ke_7(t) * \eta(t) = \int_{-\infty}^{\infty} ke_7(t-\tau)\eta(\tau)d\tau, \tag{13}$$

where $\eta(t)$ represents the free surface elevation, provided by the DTU experiments, due to an incident wave and $ke_7(t)$ represents the excitation force IRF. In this work, the excitation force IRF for mode 7 is

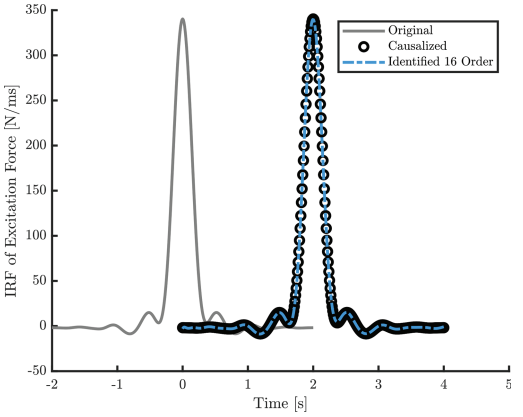

Figure 6. A comparison of excitation IRFs of original (non-parametric), causalised and parametric state space approximation for a 1-DoF DTU-OWC.

approximated by an LTI state-space system utilising the method detailed in (Guo et al. 2018). It is worth noting that the IRF of excitation force is non-causal, which means that $ke_7(t) \neq 0$ for $t<0$. Therefore, it is necessary to causalise this IRF in order to calculate a parametric approximation. The causalisation is performed by time-shifting the IRFs and the causalisation time, 't_c', of 2 [s] is used here. The resultant state space is the parametric approximation of the excitation force in the following form:

$$\begin{aligned} \dot{x}(t) &= A_e x(t) + B_e \eta_p(t), \\ fe_7(t) &= C_e x(t), \end{aligned} \tag{14}$$

where $\eta_p(t) = \eta(t + t_c)$. Figure 6 represents a comparisons between original and identified IRF for mode 7, and it is found that a parametric approximation of order 16 gives the best balance of accuracy and computational efficiency. It is important to note that the results time series calculated utilising this method are delayed by 2 [s] (causalisation time).

Figure 7 illustrates the capture-width-ratio (CWR) comparison of MU-DkIT model and experimental results for all wave periods T and $H/\lambda = 0.04$. The CWR represents the average absorbed power normalised by the available wave energy flux and is given by:

$$\bar{W} = \frac{\bar{P}}{\frac{1}{2}\rho g A^2 c_g L}, \tag{15}$$

where the length along a wave crest, L, is taken to be the chamber length along the x-axis, A is the wave amplitude, $\bar{P}$ is the averaged absorbed power, and c_g is the group velocity, respectively (Joensen et al. 2023). It is evident from Figure 7(a) that the 1-DoF time-domain MU-DkIT model compares well with the experimental results for the two-way absorption case. However, for 1-way absorption (up-/down-stroke) cases, the time-domain model tends to overestimate CWR for most wave periods, especially at and around the device resonant period, as illustrated in Figure 7(b). The overestimation observed in one-way damping cases reflects the lack of information on the whole valve arrangement and, therefore, the simple valve model (see Section 3.5) in the MU-DkIT model. As can be seen in (Joensen et al. 2023), the valve box used in the experimental testing was connected to the air volume of the OWC using flexible PVC hose attached to aluminum manifolds. No account of either the dynamics introduced by the hoses, or those of the operation of the valve, are included in the MU-DkIT model. Furthermore, the CWR is notably higher for downs-stroke absorption than up-stroke absorption, both in the model and experimental results, which is likely due to the compressibility of the air within the chamber.

To demonstrate the power absorption overestimation in one-way damping cases, Figure 8 depicts the pressure time-series comparison for down-stroke at the resonance period T = 0.82 [s]. As evidenced by Figure 8, the chamber pressure for the time-domain model is always higher than the experimental results, leading to a higher CWR observed in Figure 7(b). It is worth noting that the so-called bang-bang strategy to implement a one-way passive valve performs well to achieve zero pressure; however, it fails to capture all dynamics associated with the experimental passive valve, as shown in Figure 8, due to its relative simplicity.

5 CONCLUSIONS

In summary, this paper introduces a 1-DoF time-domain model for the DTU-OWC. Despite employing approximations for radiation and exciting forces, the model effectively captures the behaviour of the device for two-way absorption while remaining computationally efficient. In addition, the results demonstrate that, for one-way absorption, the time-domain model significantly overestimates the pressure in the OWC chamber, and hence the power absorption due to a relatively simple one-way valve model. Counter-intuitively, it is observed that the one-way damping cases can absorb more power compared to the two-way damping case for both model and experimental results. The power absorbed by the OWC in the model is proportional to the pressure in the air chamber (Kelly et al. 2015). The increase in air pressure generated in the one-way damping cases appears to compensate for the fact that power is only absorbed in one direction in these cases.

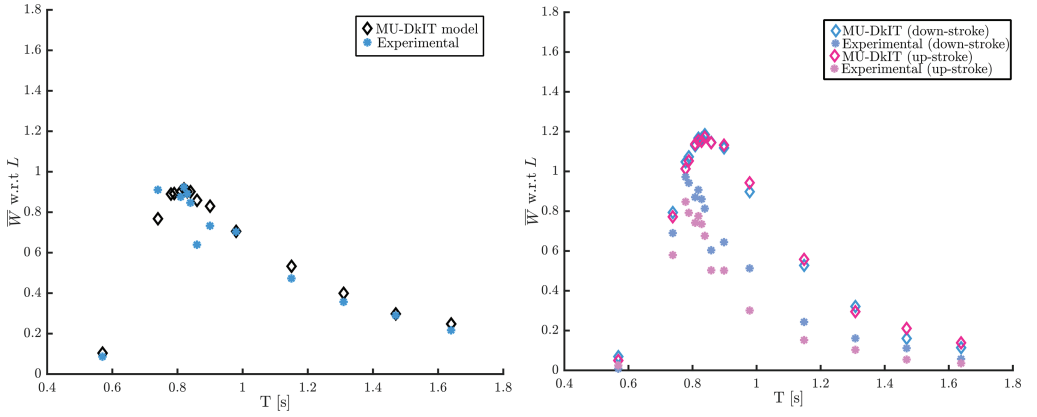

(a) Two-way absorption.

(b) One-way absorption.

Figure 7. Comparison of CWR between the time-domain model and experimental data for $H/\lambda = 0.04$.

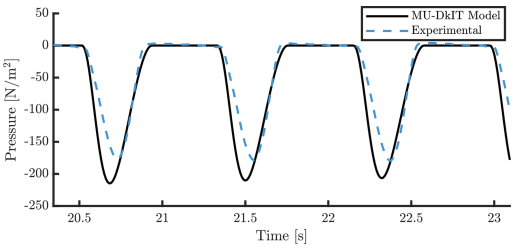

Figure 8. Chamber pressure comparison for down-stroke absorption at T = 0.82 [s] and $H/\lambda = 0.04$.

ACKNOWLEDGEMENTS

This work was supported by Science Foundation Ireland under Grant No. 21/FFP-A/8997 and through the Marine Renewable Ireland (MaREI) Centre under Grant 12/RC/2302_P2.

REFERENCES

Aerohydro Inc. (2011). *Aerohydro Multisur® User Manual*. Southwest Harbor, Maine: Aerohydro Inc.

Bingham, H. B., Y.-H. Yu, K. Nielsen, K.-H. Kim, S. Park, K. Hong, H. A. Said, T. Kelly, J. Ringwood, R. W. Read, E. Ransley, S. Brown, & D. Greaves (2021). Ocean Energy Systems wave energy modelling task 10.4: Numerical modelling of a fixed oscillating water column. *Energies 14*, 1718.

Cummins, W. E. (1962, October). The impulse response function and ship motions. Technical Report 1661, Navy Department, David Taylor Model Basin, DTNSRDC.

Dallman, A., D. S. Jenne, V. Neary, F. Driscoll, R. Thresher, & B. Gunawan (2018). Evaluation of performance metrics for the wave energy prize converters tested at 1/20th scale. *Renewable and Sustainable Energy Reviews 98*, 79–91.

Evans, D. V. (1978). The oscillating water column wave-energy device. *Ima Journal of Applied Mathematics 22*, 423–433.

Faedo, N., Y. Peña-Sanchez, & J. V. Ringwood (2018). Finite-order hydrodynamic model determination for wave energy applications using moment-matching. *Ocean Engineering 163*, 251–263.

Guo, B., R. J. Patton, S. Jin, & J. Lan (2018). Numerical and experimental studies of excitation force approximation for wave energy conversion. *Renewable Energy 125*, 877–889.

IEA (2022). OES - Ocean Energy Systems, an International Energy Agency Technology Initiative. http://www.ocean-energy-systems.org.

ISO (2022, March). Measurement of fluid flow by means of pressure differential devices inserted in circular cross-section conduits running full Part 2: Orifice plates. Standard, International Organization for Standardization, Geneva, CH.

Joensen, B., H. B. Bingham, R. W. Read, K. Nielsen, & J. B. Trevino (2023). Hydrodynamic analysis of one-way energy capture by an oscillating water column wave energy device. *Energy Reports 9*, 5306–5322.

Kelly, T. (2018). *Experimental and Numerical Modelling of a Multiple Oscillating Water Column Structure*. PhD thesis, Maynooth University. pp. 86–91.

Kelly, T., T. Dooley, J. Campbell, & J. V. Ringwood (2015). Efforts towards a validated time-domain model of an oscillating water column with control components. In *Proceedings of the 11th European Wave and Tidal Energy Conference*, Nantes, France.

Kelly, T., I. Zabala, Y. Pena-Sanchez, J. Ringwood, J. Henriques, & J. M. Blanco (2022). A post-processing technique for removing 'irregular frequencies' and other issues in the results from bem solvers. *International Journal of Marine Energy 5*(1), 123–131.

Kramer, M., J. Andersen, S. Thomas, F. Bendixen, H. B. Bingham, R. Read, N. Holk, E. Ransley, S. Brown, Y.-H. Yu, & et al. (2021). Highly accurate experimental heave decay tests with a floating sphere: A publich benchmark dataset for model validation of fluid-structure interaction. *Energies 14*, 269.

NEMOH (2017). Laboratoire de Recherche en Hydrodynamique Énergetique et Environnement Atmospherique. https://goo.gl/yX8nFu. [Online accessed: 1-July-2024].

Newman, J. N. & J. Grue (2018). *Marine Hydrodynamics*. MIT Press.

Ogilvie, T. (1964). Recent progress towards the understanding and prediction of ship motions. In *6th Symposium on Naval Hydrodynamics*.

Pena-Sanchez, Y., N. Faedo, M. Penalba, G. Giuseppe, A. Mérigaud, C. Windt, D. G. Violini, W. LiGuo, & J. Ringwood (2019). Finite-Order hydrodynamic Approximation by Moment-Matching (FOAMM) toolbox for wave energy applications. In *European Tidal and Wave Energy Conference Proceedings*, Number 1448. EWTEC.

Perez, T. & T. I. Fossen (2008). Joint identification of infinte-frequency added mass and fluid-memory models of marine structures. *Modeling, Identification and Control 29*(3), 93–102.

Reguero, B., I. Losada, & F. Méndez (2015). A global wave power resource and its seasonal, interannual and long-term variability. *Applied Energy 148*, 366–380.

Sonneborn, L. & F. Van Vleck (1964). The bang-bang principle for linear control systems. *Journal of the Society for Industrial and Applied Mathematics, Series A: Control 2*(2), 151–159.

Wamit® (2012). *WAMIT ® 7.0 User manual*. The Massachusets Institute of Technology.

Wendt, F., K. Nielsen, Y.-H. Yu, H. B. Bingham, C. Eskilsson, M. Kramer, A. Babarit, T. Bunnik., & others (2019). Ocean energy systems wave energy modelling task: modelling, verification and validation of wave energy converters. *J. Marine Science and Eng. 7*, 22.